Differential fragmentation cross sections for 7.3 GeV nitrogen ions incident on protons

John P. Wefel* and John M. Kidd
Laboratory for Cosmic Ray Physics, Naval Research Laboratory, Washington, D. C. 20375

Walter Schimmerling† and Kirby G. Vosburgh‡
Princeton Particle Accelerator, Princeton, New Jersey 08540

(Received 22 January 1979)

Differential cross sections $d\sigma/d\Omega$ for the inclusive reaction $^{14}N + p \rightarrow Z +$ anything (for $3 \leq Z \leq 6$) have been measured at six laboratory production angles ($\theta < 5°$) for 7.3 GeV nitrogen ions interacting in liquid hydrogen. The angular distributions for C, B, and Be fragments decrease sharply with increasing angle, as expected for this type of peripheral reaction. The corresponding transverse momentum (p_t) distributions for these fragments can be represented by Gaussian functions of p_t. The Li distribution appears to be non-Gaussian, suggesting one (or more) different production mechanisms. The dependence of the widths of the momentum distributions on fragment mass is not consistent with theoretical predictions, and shows some evidence for an "effective" number of nucleons which determine the fragmentation spectrum of the nitrogen nucleus. Integration of the angular distributions gives partial production cross sections which are consistent with results at higher energy. This energy-independent behavior implies that limiting fragmentation is applicable down to energies of 0.5 GeV/nucleon.

[NUCLEAR REACTIONS Relativistic heavy ions; fragmentation of 7.3 GeV nitrogen on protons.]

I. INTRODUCTION

The products of high energy, heavy ion nuclear interactions can be fragments of the projectile, fragments of the target nucleus, and nucleons (or groups of nucleons such as α particles) produced in an interaction region where projectile and target overlap. The projectile fragments emerge from the interaction that created them in a direction very close to that of the incoming primary heavy ion, with little or no change in velocity from that of the primary.[1,2]

Projectile fragmentation, most commonly referred to simply as fragmentation, shows the following characteristics[3-6]:

1. The reactions resulting in projectile fragments are due to grazing collisions.
2. The total reaction cross sections are generally independent of energy in the energy region above 300 meV/nucleon.
3. The velocity of the fragments is close to the velocity of the incident projectile, and the fragments are observed principally in the forward direction. The momentum distributions of the fragments are Gaussian in the parallel and perpendicular components, showing that they are emitted isotropically in the frame of reference of the projectile. The standard deviation of this Gaussian shape approximates a parabolic function of the beam and the fragment masses, but is independent of the target mass.
4. The probability of producing a given fragment is related to the target mass only through a geometric scale factor.
5. Geometric considerations have resulted in calculations of the total cross section as two overlapping black disks with the overlap region subtracted.[7] Saito,[8] however, analyzed the available data for inelastic cross sections, and concluded that an adequate fit is obtained by simply adding the areas of the two nuclei. A similar conclusion was reached in a calculation by Barshay.[9]

Various calculations exist for predicting the standard deviation of the Gaussian momentum distributions based on the internal energy of the projectile excited by a grazing collision,[4] but, although the predicted parabolic function is found to be a reasonable approximation, deviations persist at the 2–3 standard deviation level.

The extent to which the results of nucleus-nucleus interactions can be interpreted as due to the superposition on nucleus-nucleon or even nucleon-nucleon interactions is unclear, and constitutes one of the more interesting open questions of this field. It is thus useful to measure the fragmentation products from a nuclear projectile on a hydrogen target in order to gain a better insight into this problem. A practical advantage of such a scheme is that the fragments

are produced at approximately the beam velocity in the laboratory frame of reference; whereas, they do not have enough energy to leave the target material in the kinematically equivalent situation when a proton beam is incident on a nuclear target.

We report here a measurement of the differential cross sections for the inclusive reaction $^{14}N + p \rightarrow Z$ + anything, where ^{14}N is the incident beam, interacting in a liquid hydrogen target, and Z refers to the elements Li, Be, B, or C. The experiment was performed at the Princeton Particle Accelerator (PPA) at a beam energy of 0.52 GeV/nucleon, using a scintillation and Cherenkov counter telescope as the detector. The fragments produced at 0.25, 0.75, 1.25, 1.75, 3.00, and 4.75 degrees in the laboratory were measured within a solid angle of 0.044 msr, and the cross sections, at each angle, were obtained by subtracting a "target out" background from the "target in" measurements, after normalization and corrections. The detector provided charge resolution but no isotopic identification. Calibration studies of the detector, which yielded data on the degree of light saturation in the plastic scintillator, are discussed in the Appendix.

The transverse momentum distributions of the fragments were obtained from the differential cross sections at the different angles, assuming that the velocity of the fragments in the beam direction is the same as the projectile velocity, and using a mean isotopic mass for each element.[10] These transverse momentum distributions are compared to the results obtained a higher energy,[4] to investigate the energy dependence of fragmentation, and to the predictions of theoretical models of the process.[11] Also, the integration of the angular distribution yields partial fragmentation cross sections which are compared to the results of other experiments and to the predictions of semiempirical formulas.[10]

II. EXPERIMENTAL APPARATUS AND PROCEDURES

For this experiment the PPA[12] accelerated N^{5+} ions to 7.3 GeV with an intensity limited to 10^3–10^5 ions per second. The beam was resonantly extracted and had an energy spread $\Delta E/E \approx 2$–5% (FWHM). The PPA had an acceleration cycle of ≈50 ms; the beam was extracted in 2 ms with an RF structure of 33 ns.

Figure 1 shows the experimental arrangement. The extracted nitrogen ion beam was fully stripped in the exit window of the beam transport system; it passed through two scintillation counters and the liquid hydrogen target before entering the detector. The profile and divergence of the beam

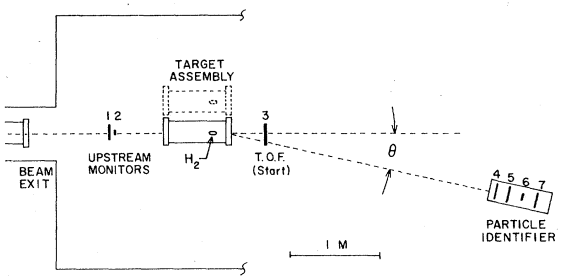

FIG. 1. A plan of the experimental area showing the beam exit window, liquid hydrogen target, TOF counter, and the particle identifier. The scintillators, Pilot B, and the Cherenkov radiator, Pilot 425, were manufactured by Nuclear Enterprises, Ltd.

were measured with a nuclear emulsion stack. The beam intensity was peaked around the centerline of the apparatus with a FWHM of ~27 mm, and displayed a divergence of ~8 mrad from a focus upstream of the apparatus. The upstream monitor scintillator (#2) was used to select the central ~20% of the beam distribution for this experiment.

The liquid hydrogen target (LHT) was enclosed in an evacuated cylinder with 0.025 cm thick Mylar end windows. The liquid hydrogen was contained in a cylindrical Mylar flask 6.61 cm in length with molded hemispherical end caps of 0.008 cm thick Mylar. The temperature and vapor pressure of the hydrogen were monitored continuously, and the temperature was regulated by a heating resistor. The target was mounted to be moved into and out of the beam with a reproducibility of position in the beam of ±0.05 cm. The target assembly presented approximately 0.5 g/cm² of liquid hydrogen and ~ 0.09 g/cm² of Mylar on the beam. With the target assembly removed from the beamline, an additional 0.09 g/cm² of air is placed into the path of the particles, making the target "empty" configuration approximately equal for fragmentation to the target "out" beamline.

The elements of the detection system, shown schematically on Fig. 1, are described in Table I in which the "counter" column refers to the numbers on Fig. 1. The upstream counters, 1 and 2, monitored the number of incident particles and selected the beam events. Counters 3 and 6 comprised the time-of-flight (TOF) telescope, and scintillators 4 and 5 were designed to measure the energy lost by each event. The disc counter (6) restricted the solid angle of the telescope to 0.044 ±0.001 msr, and the Cherenkov detector (7) was used to select particles with velocity $\beta \gtrsim 0.63$. Detector elements 4–7, the particle identifier, were moved as a unit to the various

TABLE I. Counter descriptions.

Counter	Purpose	Dimensions (cm)
1	Upstream monitor	$12.5 \times 12.5 \times 0.25$
2	Monitor and beam selection	0.3×0.9 diam. disc
3	TOF (start)	$12.5 \times 12.5 \times 0.3$
4	First dE/dx	$12.5 \times 12.5 \times 0.9$
5	Second dE/dx	$12.5 \times 12.5 \times 0.9$
6	TOF (stop) and geometry	0.3×1.9 diam. disc
7	Cherenkov	$12.5 \times 12.5 \times 0.6$

angles.

The efficiency, as a function of photomultiplier voltage, was measured for each counter with both cosmic-ray μ-mesons and a low-intensity nitrogen beam. The operating voltages were set in the middle of the resulting plateaux of the efficiency curves. Counters 4 and 5 each had two light pipes giving two output signals (referred to as a and b). The outputs with the better resolution, $4b$ and $5b$, were used for pulse height analysis, and signals $4a$ and $5a$ were employed to monitor the detector performance.

The electronic logic for data acquisition is shown schematically in Fig. 2. The solid boxes containing numbers on Fig. 2 show coincidences which provided information on detector efficiency and performance or on the beam characteristics. The 1 [2] rate refers to a coincidence between counter 1 and a delayed signal from counter 2. The delay corresponds to the time between beam pulses (≈ 33 ns); the 1 [2] rate is related to the average number of beam particles per pulse.

Acceptable events were defined by the logic $1264b5b$, which constituted the "event" trigger.

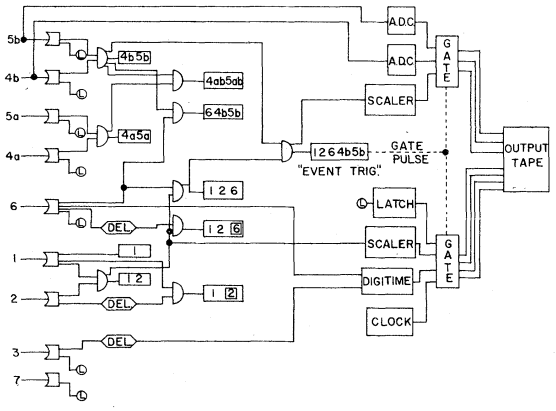

FIG. 2. The logic diagram for the experiment. Boxes containing numbers represent scaler rates recorded for each run. The magnetic tape readout system is indicated on the right-hand side of the figure.

Once an acceptable event was recognized, the "event" trigger enabled a gate for readout onto the magnetic tape.

III. CALIBRATION

Before data acquisition was begun, the detector counters were calibrated in the nitrogen beam to determine their efficiency, resolution, and time response. By fitting Gaussian curves, counters $4b$ and $5b$ displayed pulse height resolutions of 6% and 9% (FWHM), respectively; counters $4a$ and $5a$ each had a FWHM in excess of 10%. For the TOF system a resolution in energy of ~30% was obtained (due to the short baseline over which the TOF was measured). This was not sufficient to detect small changes in energy, but it did provide a means of rejecting background triggers.

Test runs were conducted with the detector positioned at a small angle to the beam and a thin metal slab in the beam as a target for fragmentation. The event trigger was 1246 for these runs, and only particles in the central portion of the TOF peak were accepted for analysis. This provided a sample of all charges for which the efficiency of each counter was measured utilizing the pattern register. All counters displayed an efficiency of 100% for $Z > 2$ particles except for the Cherenkov detector, whose efficiency decreased with charge from 100% for nitrogen and carbon to 88% for lithium.

These data were also used to determine the response curve of the Pilot B scintillator, discussed in the Appendix. The observed scintillator saturation is in general agreement with previous measurements and is not severe enough to cause any misidentification of the fragments as illustrated by the uncorrected pulse height spectrum for counter $4B$ shown on Fig. 3(a). Protons and most α particles were excluded by the discriminator thresholds. On Fig. 3(a), the peaks for lithium and beryllium events are broader than expected considering only photoelectron statistics.[13] Instrumental effects may account for some of the width, but much of the broadening appears to be

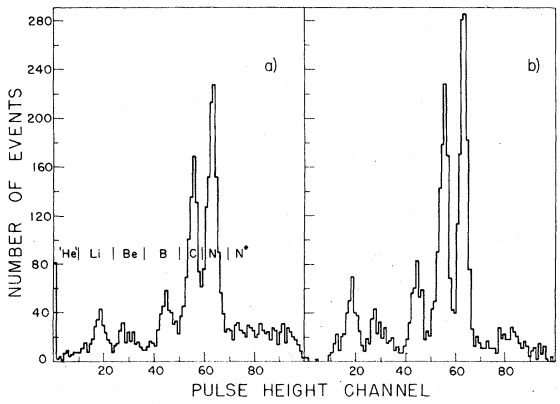

FIG. 3. Pulse-height spectrum observed in counter 4*b* at a production angle of 0.75°. Raw data are shown on part (a) with charge intervals indicated. Part (b) gives the corrected correlated spectrum, for the same data, normalized to the same number of events as part (a).

due to a kinematical effect in the fragmentation process. In the projectile rest frame, a given type of fragment may be emitted into either the forward or backward hemisphere. In the laboratory, these events have a small difference in velocity, and consequently, a variation in the amount of energy deposited in the scintillator. This leads to a broadening of the peaks which is most evident for lithium and beryllium as these fragments are approximately half of the mass of the incident beam.

A second feature of Fig. 3(a) is the presence of many events in pulse-height channels higher than the nitrogen peak. These are assumed to represent multiple particles in the detector ("pile up") within the system resolving time. This interpretation is consistent with the following experimental observations: For the same angular position, the fraction of "pile-up" events increases with the intensity of the nitrogen beam. Also, for runs in the direct beam near 0°, the "pile-up" spectrum shows a peak characteristic of two nitrogen ions recorded simultaneously. Finally, "pile-up" events are absent for runs at large production angles, such that the edge of the direct beam is removed from the detector.

Four types of multiple events are considered: First, a particle (either beam or fragment) accompanied by a nitrogen ion. This class of event appears in the pulse-height spectrum above the nitrogen peak, and will produce corresponding signals in counters 4 and 5. The distribution of these "pile-up" events mirrors the distribution of events in the lower pulse-height channels; these events were thus assigned to the various charge peaks.

Second, two separately produced fragments recorded simultaneously. For the low beam rate in this experiment, the probability of this occurrence is negligible.

Third, a beam or fragment particle recorded along with background radiation such as low energy protons, α's, or neutrons. This background might arise from interactions of the beam with the framework around the detector or other extraneous material along the beam line. Depending upon the energy of the background radiation this third type of "pile-up" may appear anywhere in the pulse-height spectrum, but will not necessarily produce the same signal in counters 4 and 5, which together comprise about 2 g/cm^2 of material. Thus, these events can be eliminated by requiring a correlation between the signals in counters 4 and 5, as described in the following section.

Fourth, two particles being produced in the interaction process. An example is the production of ^{8}Be, which decays before reaching the detector into two α particles. In most interactions, the particles in the final state are well separated in angle and only one particle is contained within the solid angle of the detector. However, in the case of radioactive ^{8}Be, the decay energy is not sufficient to separate the two α particles, and these events appear at the location of the lithium peak in the pulse-height spectrum. It was not possible to eliminate this effect directly during the analysis, and a correction to the final cross sections was necessary.

IV. DATA ANALYSIS

The data set for the measurement of the differential cross sections consisted of 15 runs, each with the target in and the target out of the beam line, at six separate production angles between 0 and 5 degrees to the beam direction. A typical run consisted of 3000 to 20 000 events at a given angle. For each angular position, the differential cross section was obtained from

$$\frac{d\sigma}{\sigma\Omega}(Z,\theta)=\left[\frac{N^i(Z,\theta)}{M^i}-\frac{N^o(Z,\theta)}{M^o}\right]\frac{1}{\Delta\Omega}\,\frac{A}{\mathfrak{N}_0}\,\frac{1}{\rho\Delta X}, \tag{1}$$

where $N(Z,\theta)$ is the number of fragments of charge Z at the angle θ, and the superscripts i and o refer, respectively, to runs with the target *in* and the target *out* of the beam, M is the number of incident beam particles, $\Delta\Omega$ is the solid angle subtended by the detector, A is the atomic weight of the liquid hydrogen, $\mathfrak{N}_0$ is Avogadro's number, ρ is the mean density of the liquid hydrogen during the run, and $\Delta X = 6.61 \pm 0.07$ cm is the mean path

length in the liquid hydrogen along the beam direction.

A. Determination of $N(Z,\theta)$

The number of fragments of each charge, at each angle, $N(Z,\theta)$, was obtained from pulse-height spectra in counters $4b$ and $5b$ that satisfied the hard-wired trigger logic ($124b5b6$), fired the Cherenkov counter, and fell in the TOF window. The pulse-height spectra were divided into charge intervals, as shown in Fig. 3(a), and a further selection was made of events that fell into corresponding charge intervals in the pulse-height spectra of both counters $4b$ and $5b$. Small changes in the definition of these charge intervals did not change the number of events by more than 2% in the worst case.

The distribution of the events thus selected was fitted to a Gaussian shape, and the appropriate areas under the tails of the distribution were added, with consideration for overlap of adjacent charge intervals. This number was then corrected, for each charge, for nuclear interactions in the ~2 g/cm^2 of scintillator material (4%–6%, depending on fragment type).[7,14,15] Estimates of fragmentaion probabilities obtained from semiempirical cross section formulas[10] were used to calculate the fraction of nuclear interactions resulting in events already included in the previous selection. This correction was found to be less than 1% for all charges. The overlap and interaction corrections contributed between 10% and 15% to the number of events, depending on angular position and charge resolution.

Let the events selected according to the above procedure be denoted by $n_c(Z)$. These events must be further corrected for effects due to multiple particles and the nonunity Cherenkov counter efficiency in order to obtain $N(Z,\theta)$. A pulse-height spectrum of $n_C(Z)$ is shown on Fig. 3(b), normalized to the same number of events as in Fig. 3(a). The presence of events due to helium in Fig. 3(a) shows that the discriminator thresholds were sufficiently below the lithium channel so that no loss of real lithium particles occurred. The efficiency of the selection procedure for $n_C(Z)$ may be seen by comparison with Fig. 3(b), where no significant contamination by helium remains.

The multiple particle events above the nitrogen peak, illustrated in Fig. 3(b), were divided among the various charges in proportion to the fraction of $n_C(Z)$ in the total spectrum, after corrections for the ~5% difference in solid angle between counters 4 and 5 (which results in different geometries for multiple event detection) and for nuclear interactions. Let the number of multiparticle events assigned to each charge be $n^*(Z)$. Then the number of events of charge Z obtained is $n_C(Z)+n^*(Z)$.

Multiple events consisting of a fragment or beam particle accompanied by background, and any events in possible non-Gaussian tails of the distributions for each charge are not included in $[n_C(Z)+n^*(Z)]$. This results in a loss of otherwise legitimate contributions to $N(Z,\theta)$ of the order of 5%. In order to correct for this loss, $n_C(Z)+n^*(Z)$ was normalized to the total number of events. Let ϵ_Z be the Cherenkov counter efficiency. Then

$$N(Z,\theta)=[n_C(Z)+n^*(Z)]/h\epsilon_Z\ , \tag{2}$$

where the normalization factor, h, is given by

$$h=(1/n_0)\sum_{Z=3}^{Z=7}[n_C(Z)+n^*(Z)], \tag{3}$$

and n_0 represents the total number of particles with $Z>2$ that satisfy the trigger logic, and are counted by the Cherenkov detector.

B. Determination of M

The normalization, M, was obtained from the recorded number of counts in the beam telescope, (12), after correction for accidental coincidences between counters 1 and 2, not related to the beam. The number of counts from counter 1, N_1, was recorded for each run. Assuming that the rate of counter 2 is approximately the same as the coincidence rate between the counters, the number of accidental counts for a run consisting of N_s spills (each of which is 2 ms in duration) was calculated according to

$$(12)_{\rm acc}=(12)\times[1-\exp(-R_1\Delta T)], \tag{4}$$

where $\Delta T=250$ ns is the length of the output discriminator pulse from counter 1, and $R_1=N_1/(2\times10^{-3}\ \text{ns})$ is the counting rate in counter 1.

For most of the runs reported here, the number of accidental coincidences was only a few percent of the total.

C. Other parameters

The density of the liquid hydrogen in the target used for each run was calculated from the average temperature and vapor pressure of the liquid.[16] The hydrogen density varied by less than 10% over the series of runs composing this data set. The mean thickness in the beam direction of the column of liquid hydrogen was taken as the distance between the intersections of the hemispherical end caps with a cylinder of cross section equal to one-half the area of the beam spot accepted by counter 2. This was found to be 6.61 ± 0.07 cm, with the uncertainty determined by the curvature

of the flask end caps over the selected portion (0.95 cm diameter of counter 2) of the beam.

The angular position for each run was determined from the positioning of the detector and the beam, relative to the center line of the apparatus. Beam drift, due to small changes in the quadrupole magnets in the beam transport system, was monitored by the ratio $\frac{12^6}{12}$ which gives, for runs at zero degrees, the fraction of the beam incident on the disc of counter 6. Only one shift in the beam position was observed throughout the experiment.

D. Consistency checks

Several tests were applied to the experimental data to check for consistency in analysis and normalization. First, if the analysis and normalization are correct, the values of $d\sigma/d\Omega$ obtained by subtracting two presumably identical runs should be zero within the experimental uncertainties. Thus null-cross-section test was applied to "target-in" runs at small angles, and $d\sigma/d\Omega$ values for two runs at 0.25° are shown in Table II. The cross sections are consistent with zero within the uncertainties. For the results in Table II, the χ^2 confidence level is ~70%, due principally to the carbon cross section which may be influenced by the large nitrogen peak recorded in these runs near zero degrees. The confidence level is much higher for the remaining fragments.

A second test was applied to the "nitrogen" events which should show a cross-section dependence on laboratory scattering angle given by the Rutherford scattering formula.[17] Figure 4 shows the differential cross section for relativistic Rutherford scattering plotted over the data points measured in this experiment. The data are in excellent agreement with the calculated curve.

As noted above, "target out" (as opposed to "target empty") runs were used for background subtraction, since the amount of material in the beam was the same in each case. A data run was made with an empty target to verify this, and the results were equal to those of a "target out" run within the estimated measurement uncertainties.

TABLE II. Null-cross-section test at $\theta = 0.25°$.

Fragment	$d\sigma/d\Omega$ (mb/sr)
Carbon	5.3 ± 3.7
Boron	0.1 ± 1.3
Beryllium	0.4 ± 1.4
Lithium	0.3 ± 0.9

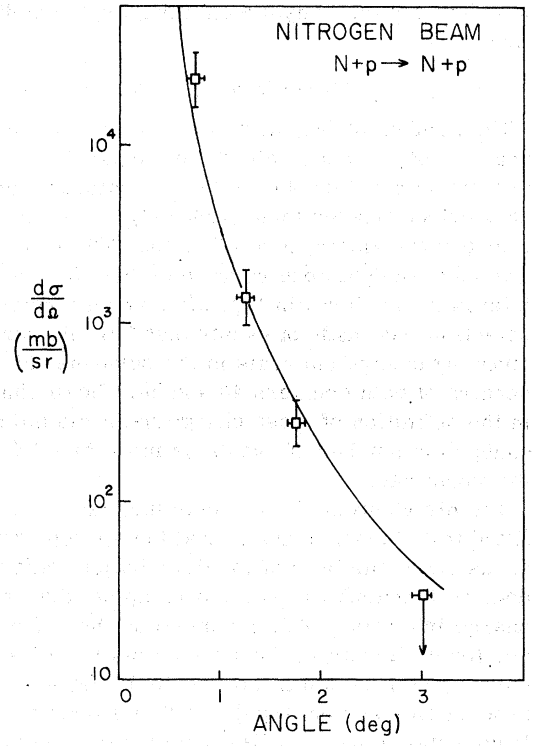

FIG. 4. The angular distribution of the nitrogen data plotted over the calculated relativistic Rutherford scattering cross section for > 0.5°.

V. ERROR ANALYSIS

The main source of error in the differential cross sections is the statistical uncertainty introduced by the "target in-target out" subtraction, followed by the errors in $N(Z, \theta)$, M, θ, and ρ. The solid angle, $\Delta\Omega$, and the thickness of the column of liquid hydrogen are known accurately, and their errors contribute less than 1% each to the final uncertainty. Table III lists the sources of error, an estimate of the absolute magnitude of each, and the contribution of each to the final uncertainty in $d\sigma/d\Omega$.

The statistical uncertainty in the number of events collected for each charge group varies from about 5% to 20%, depending upon the fragment and the angle. Few lithium fragments were observed at small angles, and few nitrogen particles were found at the larger angles. Uncertainties in the mean and the width of the Gaussian distributions introduce an error into the correction for distribution overlap. The corrections for interactions in the detector are based upon cross-section estimates which are accurate, on the average, to 20%. However, since only about 5% of the incident particles undergo a nuclear interaction, these corrections contribute negligibly to

TABLE III. Error estimates.

Quantity	Source	Uncertainty	Contribution to final error
$N(Z,\theta)$	Statistical	3–15%	5–20%
	Corrections	4–8%	2–5%
	Overlap	3–7%	1–2%
	Interactions	$\lesssim$5%	$\lesssim$2%
	$\check{C}$ Efficiency	$\lesssim$2%	$\lesssim$1%
M	Statistical	$\lesssim$1%	$\lesssim$0.5%
	Correction	$\lesssim$50%	$\lesssim$1%
ρ	Fluctuations	$\lesssim$1%	$\lesssim$1%
θ	Positioning	±0.05°	···

the final uncertainty. Similarly, the Cherenkov efficiency was only a small correction.

The uncertainty in normalization M is derived from a combination of the statistical uncertainty in (12) and the error in the correction for accidental coincidences. The density of the liquid hydrogen fluctuated a small amount throughout each run. This variation was monitored, and the uncertainty in the mean density was found to be $\leq 1\%$.

Detector and beam positioning combine to give an uncertainty of ± 0.05° in the angular position for each run. A possible systematic error may result from a difference in angle between the target-in and target-out runs, which were nominally at the same position. As a precaution, data were taken at zero degrees before and after each set of runs at large angles. In addition, all "target-out" data were plotted versus angle to look for any suspicious runs, and none were found, thereby eliminating concern about beam shifts.

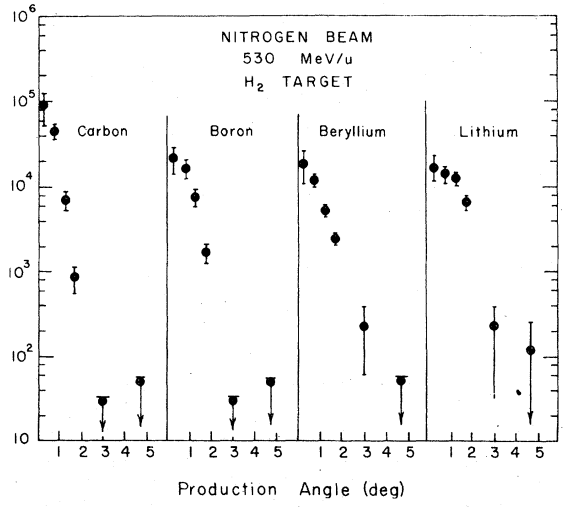

FIG. 5. The angular distributions of the fragments carbon, boron, beryllium, and lithium.

VI. RESULTS AND DISCUSSION

A. Angular and transverse momentum distributions

The differential cross sections, $d\sigma/d\Omega$, are plotted as a function of the production angle in Fig. 5. The angular distributions are sharply peaked in the forward direction, as is characteristic of peripheral processes with small momentum transfer. The Be and Li distributions are somewhat broader, and the lithium distribution shows a shoulder at small angles. These distributions are consistent with the results of a recent study of 2-GeV/nucleon ^{16}O interactions in nuclear

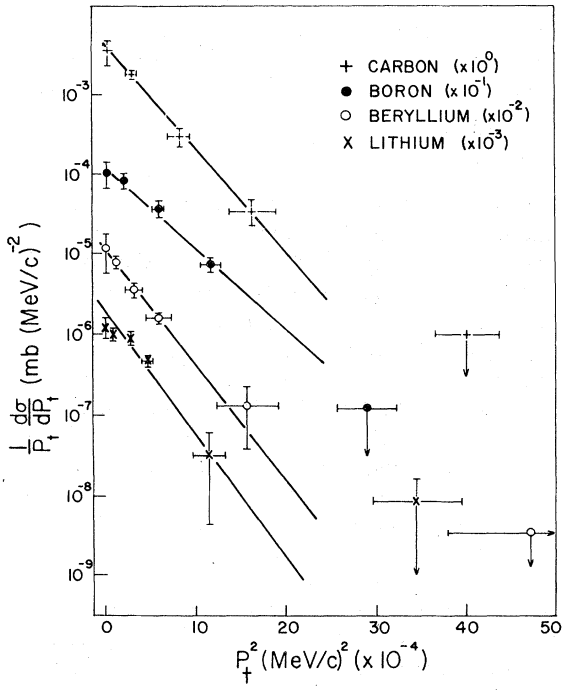

FIG. 6. The transverse momentum distribution for the fragments, including solid curves, showing the least-squares fit to the data with $p_t \leq 500$ MeV/c. (See text for details.)

TABLE IV. The widths δ in MeV/c of the momentum distribution.

Beam	Energy (GeV/u)	C	B	Be	Li	Reference
^{14}N	0.5	130 ± 4	147 ± 9	133 ± 3	124 ± 15	This experiment
^{12}C	1.05	115 ± 9	116 ± 10	138 ± 7	145 ± 8	4
^{12}C	2.1	124 ± 8	113 ± 4	140 ± 3	138 ± 5	4
^{16}O	2.1	120 ± 4	167 ± 5	166 ± 5	152 ± 5	4
^{16}O	2.0	~140				5

emulsion,[5] where the lithium distribution was found to be considerably wider than expected, while the momentum distribution of carbon was in agreement with the present results. Our data are also consistent with an explanation of the ^{14}N fragmentation cross section obtained by Heckmann *et al.*[2] (see below) as due to an underestimate of the width of the angular distribution. Agreement with nuclear emulsion data should not be surprising since the shape of the projectile fragmentation distributions has been found to be independent of target.[4]

It is useful to present the data in terms of the quantity $(1/p_t)d\sigma/dp_t$, where it is expected that[4,5]

$$(1/p_t)d\sigma/dp_t \propto \exp[-\tfrac{1}{2}(p_t/\delta)^2] . \quad (5)$$

The transverse and longitudinal momenta of the fragments were not measured directly, but can be calculated from the beam momentum and the measured angle, if it is assumed that the longitudinal velocity of the fragments is equal to the velocity of the beam, as

$$p_t = \left(\frac{A_f}{A_B}\right) p_B \tan\theta , \quad (6)$$

where $A_B = 14$ is the mass of the beam nuclei, p_B is the beam momentum, and A_f is the fragment mass. A_f was calculated as the mean mass for each element, weighted by the fragmentation parameters for each isotope obtained from the semiempirical cross section model.[10]

The transverse momentum distribution is shown on Fig. 6, and the lines give the least-squares fit of Eq. (5) to points with $p_t \leq 500$ MeV/c. The widths of the Gaussians, δ, are collected in Table IV, along with results obtained at higher energies, averaged over the isotopic distribution. The higher energy results of Ref. 4 are, furthermore, widths of longitudinal momentum distributions, found by the authors to be equal to the transverse momentum distributions at the 10% level. The results for carbon and Be seem to be in reasonable agreement. The width for boron seems to be intermediate between that reported in Ref. 4 for carbon and oxygen beams. The forced straight-line fit to the lithium momentum distribution in Fig. 6 masks the effect of the shoulder, yielding a width more comparable to results reported in Ref. 4 for ^{10}Li. If the shoulder slope is weighted more in the fit, a larger width results. The data suggest the presence of nuclear structure effects, as also noted elsewhere,[4,8] but are insufficient to provide further insight into their nature.

The widths of the distributions given in Table IV have been predicted, on the basis of general statistical principles,[11] to be function of the mass of the beam A_B, and of the fragment, A_f:

$$\delta^2 = 4\delta_0^2 A_f (A_b - A_f)/A_b^2 , \quad (7)$$

where δ_0 is a constant of the model related to the nuclear Fermi momentum. Modifications to this relation, based on a two-step ablation-abrasion model[18] have been calculated. These calculations result in anisotropies yielding widths of the transverse momentum distribution greater than those of the corresponding longitudinal momentum distribution by approximately 10%. Such effects are of the order of magnitude of the errors in the

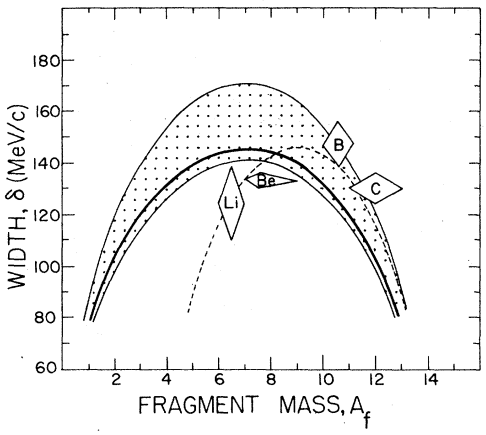

FIG. 7. The dependence of the widths, δ, on the fragment mass for ^{14}N fragmentation. Data points are indicated as diamonds. Extrapolation of the results measured at higher energies gives the stippled region, and the solid line represents a fit of the present data to Eq. (7). The dashed curve is the prediction obtained by assuming that an "effective" number of nucleons interacts, as described in the text.

measured widths, and need not be of concern here.

The widths obtained in this experiment are plotted as a function of fragment mass in Fig. 7. The stippled region shows the range of values expected, using Eq. (7) to represent the higher energy data, with δ_0's given by Ref. 4. The upper limit of this region corresponds to the results quoted for 2.1-GeV/nucleon ^{16}O, and the lower limit corresponds to 1.05-GeV/nucleon ^{12}C data.[4] The experimental values obtained in this experiment are indicated as diamonds centered on the mean mass of the fragments for each element, as determined from semiempirical cross-section formulas.[10] The lateral extent of the diamonds denotes the mass range covered by the most abundant isotopes. The solid black curve is a fit of Eq. (7) to the present data, yielding a value of $\delta_0 = 146 \pm 6$ MeV/c.

It can be seen in Fig. 7 that Eq. (7) only agrees with the data within 2–3 standard deviations. This is consistent with the observation of Greiner *et al.*[4] that, while Eq. (7) is an adequate qualitative guide to the behavior of the distribution widths at high energies, discrepancies of the same order of magnitude, as noted here, exist, ascribed in Ref. 4 to nuclear structure effects. Deviations from the parabolic form of Eq. (7) are predicted by a cluster substructure model of the fragmenting nucleus[19]; however, these deviations are considerably smaller in magnitude than the observed ones.

The existence of clusters in the projectile may be thought of as a "core" of spectator nucleons that do not participate in the interaction, while only an "effective number" of nucleons interact with the target. Such an idea is not new, and has been employed successfully to interpret other aspects of peripheral interactions, such as pion production by heavy ions.[20,21] For the present data, this idea can be explored by replacing the masses of the beam and the fragment in Eq. (7) by $(A_f - n)$ and $(A_b - n)$, where n is the mass of the putative core. Adopting $\delta_0 = 146$ MeV/c, a value of $n = 4.1$ is obtained. It is tempting to speculate on whether this value of n is indicative of a spectator α-particle core in the fragmenting projectile. The broken curve on Fig. 7 has been calculated for $n = 4.0$, and seems to provide a somewhat better fit to our data.

B. Partial cross sections

The partial cross sections for the production of each of the fragments were determined by integrating the angular distribution, and the results are given in Table V. The values for lithium and beryllium have been corrected for multiple-particle events, using calculated cross sections for ^8Be and ^9B production[10] and estimates of the small contributions from total breakup events. The corrections were -10 ± 3 mb and -2 ± 1 mb, respectively. Also shown in Table V are the results from other experiments for ^{12}C, ^{14}N, and ^{16}O fragmentation at similar and higher energies. Entries 2–5 give results from experiments at the Bevatron, which measured the forward fragmentation products (within ± 12.5 mrad of the beam direction for lines 2, 3, and 5; ± 4 mrad for the early data in entry 4) for a variety of projectiles. The results given for hydrogen were obtained by CH_2-C subtraction. Note that for the data listed in row 4, some of the isotopic cross sections for hydrogen were not reported explicitly. These were obtained by scaling the carbon target results by the factor of 0.62 given by the authors.[2] The following two lines, 6 and 7, show the results obtained by the Orsay group[22–25] from mass spectrometer studies of carbon and oxygen targets irradiated by 600 MeV protons (corresponding to approximately the same relative velocity between target and projectile, as in this experiment). The values quoted on line 8 are derived from the

TABLE V. Production cross sections in mb.

Entry	Beam	Target	Energy (GeV/u)	Fragments C	B	Be	Li	Reference
(1)	^{14}N	p	0.5	59 ± 10	28 ± 4	23 ± 3	31 ± 5	This experiment
(2)	^{12}C	CH_2-C	1.05		50 ± 3	17 ± 1	23 ± 2	3
(3)	^{12}C	CH_2-C	2.1		48 ± 5	19 ± 1	26 ± 2	3
(4)	^{14}N	CH_2-C	2.1	39 ± 6	20 ± 3	8 ± 2	~7 ± 1	2[d]
(5)	^{16}O	CH_2-C	2.1	66 ± 5	26 ± 5	16 ± 1	25 ± 3	3
(6)	p	^{12}C	0.6			19 ± 2	29 ± 3	24,25
(7)	p	^{16}O	0.6		37 ± 13[a]	10 ± 2	24 ± 5	22,23
(8)	^{14}N	p	0.4	77 ± 23	50 ± 15	29 ± 9	22 ± 7	10[b]
(9)	p	^{14}N	0.6		40 ± 12[a,c]	20 ± 6[c]		26,27

[a] Contains production of $^{10,11}C$ as well as $^{10,11}B$.
[b] Semi-empirical calculations.
[c] Contains estimated value for one or more isotopic cross sections.
[d] Data apply only to 4.5 mrad cone centered at 0°.

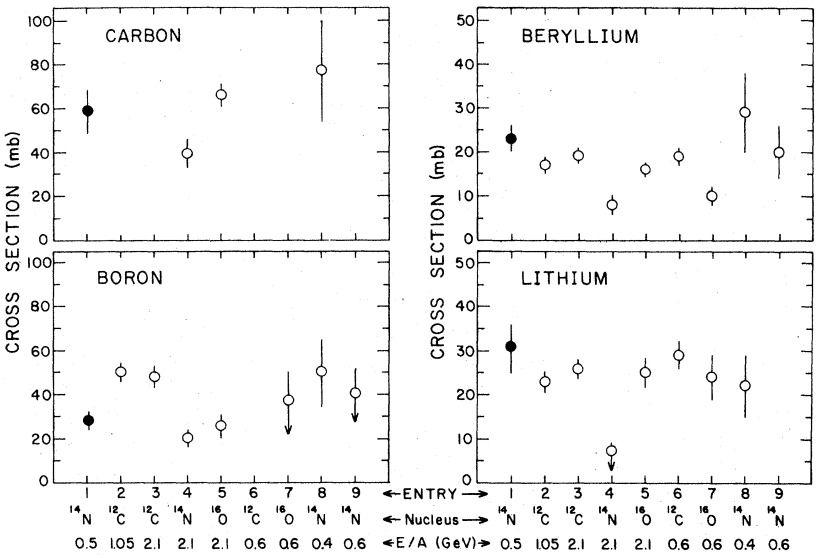

FIG. 8. The partial cross sections for the production of the fragments C, B, Be, and Li from Table V are plotted for comparison. The table entry number, the fragmenting nucleus, and the beam energy are indicated. The results from the present experiment are shown in position 1.

semiempirical equations,[10] with parameters that include fits to high-energy data. A standard error of 30% has been assigned to these calculated cross sections. There are no other measurements of the complete fragmentation spectrum of ^{14}N, but there have been measurements of the production cross sections for selected isotopes in ^{14}N fragmentation reactions (see the compilation of data given in Ref. 10). The final line of Table V gives results from one set of experiments for which values of the unmeasured isotopic cross sections were estimated from other data.[26,27]

The results summarized in Table V are plotted on Fig. 8 for easier comparison. The horizontal scale refers to the entries in Table V, and, in addition, the beam energy and the nucleus which fragments are indicated. It is evident that the data for 2.1-GeV/nucleon ^{14}N fragmentation[2] are systematically low. This was noted by the authors, and interpreted as due to the small acceptance angle of their apparatus. The broader angular distribution of lithium, as noted above, would account for the low value shown in Fig. 8.

The results given in Table V and on Fig. 8 appear to be constant within ~20% over the entire energy range 0.5 to 2.1 GeV/nucleon. The results suggest energy independence in the fragmentation process above 0.5 GeV/nucleon, which would support the hypothesis of "limiting fragmentation" advanced to explain the behavior of composite particles in high-energy interactions.[2]

VII. CONCLUSIONS

The angular and transverse momentum distributions measured in this experiment are consistent with the assumptions that these fragmentation reactions are mainly peripheral in character, and that the fragments are emitted isotropically in the projectile frame of reference. The lithium fragments may be an exception to this general behavior, perhaps due to an additional or different production mechanism. The partial cross sections obtained by integrating the measured angular distributions are generally consistent with other experiments within the uncertainties. Comparison of the present results with data at 1.05 and 2.1 GeV/nucleon seems to indicate that fragmentation is energy independent (at ~20% uncertainty level), supporting evidence for the idea of limiting fragmentation at energies as low as 0.5 GeV/nucleon. The widths of the momentum distributions found in this experiment do not fit the expected parabolic form, and provide further indication of the importance of nuclear structure effects.

We thank, particularly, Dr. M. G. White and the staff of the Princeton Particle Accelerator, whose efforts made this experiment a reality. We are also indebted to Dr. M. M. Shapiro, for his help and encouragement, and to the Naval Research Laboratory and the Fannie E. Rippel Foundation for timely financial support. The U. S. Atomic Energy Commission supported the construction and operation of the PPA for many years. Thanks are also due to G. Woods, for excellent technical assistance on all aspects of this experiment, to Dr. C. H. Tsao for assistance in data analysis, and to K. de Angelis, L. Beahm, J. Fennimore, and G. Peace for experimental assistance. Helpful discussions on various aspects of high-energy fragmentation with M. M. Shapiro, R. Sil-

berberg, H. Heckman, P. Lindstrom, D. Greiner, J. Adams, G. Mueller, and A. Goldhaber are gratefully acknowledged.

APPENDIX A: PILOT *B* SCINTILLATOR RESPONSE

In the course of this experiment, it was necessary to measure the detailed response of the Pilot *B* scintillator to the particles under consideration. This was done by selecting a sample of events of each charge at the beam velocity (see text for configuration), and by employing nitrogen beam particles, whose energy was reduced by known amounts in measured thicknesses of graphite absorbers. The scintillator light output was recorded by a pulse-height analyzer, and the energy deposited in the scintillator for each particle or absorber configuration was computed from range-energy tables.[28]

The effect of the photomultiplier tube and associated electronics was measured separately by coupling a fast-rise-time light pulser to the center of the scintillator, and employing calibrated neutral density filters to give light pulses of varying intensity. This relative light scale was related to energy loss values by exposing the scintillator, both to a ^{90}Sr-^{90}Y β-particle source and to cosmic-ray muons, and subsequently fitting the measured spectra to the known β-particle and muon distributions. These two scale calibrations agreed to better than 10%. Each data point was converted into the signal resulting only from the scintillator by unfolding the saturation due to the PM tube and electronics. The results are given on Fig. 9. Most of the saturation in output was due to the scintillator material itself.

Scintillator saturation has been widely studied with low energy particles[29-32] and, to a lesser extent, with high energy, penetrating particles.[13,33,34] Badhwar *et al.*[33] summarized much of the earlier data, and showed that the response of the NE-102 scintillator was adequately described by the equa-

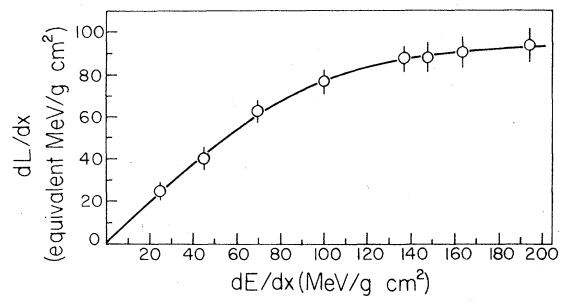

FIG. 9. The response of Pilot *B* scintillator, showing the specific light output as a function of energy loss rate for counter 4*b*. The curves represent fits to the data (see Appendix).

TABLE VI. Scintillator response parameters.

Scintillator	dE/dx (MeV/g/cm^2)	S	Kb (MeV/g/cm^2)$^{-1}$	C (MeV/g/cm^2)$^{-2}$	Comments	Reference
Pilot *B*	0–200	1.04 ± 0.19	$(1.2 \pm 0.2) \times 10^{-3}$	$(2.8 \pm 0.5) \times 10^{-5}$	Raw data	This work
Pilot *B*	0–200	1.03 ± 0.28	$(8 \pm 2) \times 10^{-4}$	$(2.7 \pm 0.7) \times 10^{-5}$	Unfolded data	This work
NE 102	<100	1.02	$\sim 1.0 \times 10^{-2}$	0	Summary of data	33
NE 102	⩾100	1.02	7.8×10^{-3}	-7×10^{-6}	C^{12}, O^{16} Cosmic rays	33
NE 102	2–1300	1.05[a]	$\sim 10^{-3}$	0	Cosmic rays @ $\beta \sim 1$	13
Pilot *Y*	<350	1.05[a]	3.9×10^{-3}[a]	0	C^{12} Cosmic	34
Pilot *Y*	<500	1.05[a]	3.6×10^{-3}[a]	0	O^{16} rays	34
NE 102	High	...	$(3.5–7.5) \times 10^{-3}$	0	Stopping protons	29
Pilot *U*	>1000	2.07	4.4×10^{-4}	0	C^{12} Stopping	32
Pilot *U*	>1000	1.79	2.4×10^{-4}	0	O^{16} heavy ions	32

[a] Values inferred from graphical data assuming $C = 0$.

tion[35,36]

$$\frac{dL}{dx} = \frac{S\,dE/dx}{1 + kb\,dE/dx + C(dE/dx)^2} \quad , \qquad \text{(A1)}$$

with $C \cong 0$ for values of dE/dx less than about 100 MeV cm^2/g. Including larger energy loss values, $dE/dx > 100$ MeV cm^2/g, the specific light output per unit path length, dL/dx, requires a value of $C = -7\times10^{-6}$ MeV cm^2/g)$^{-2}$. Values for the constants S, kb, and C, obtained by fitting our data on Fig. 9, are given in Table VI. The first line gives the results for the raw data, Pilot B scintillator plus PMT and associated electronics. A comparison with the unfolded data (second line on Table VI), shows that only a small amount of saturation was introduced by the photomultiplier tube and electronics. The present data cannot be fitted, acceptably, with a value of $C = 0$, and the value of the constant C inferred is positive rather than negative. Further, the value of the quenching factor, kb, found in this experiment, is significantly less than that found in Ref. 33 (as given on the third and fourth lines of the Table).

The remaining entries in Table VI give values for the constants S, kb, and C derived from other studies of the response of plastic scintillators. Note that the data divide themselves into two groups: results derived from high-energy particles, in particular, cosmic rays, and data derived from low-energy stopping protons or heavy ions. Our results are in approximate agreement with the data for relativistic cosmic rays in the NE 102 scintillator,[13] but give a smaller kb parameter than the results for cosmic rays in the Pilot Y scintillator.[34] It should be noted that the values quoted in Table VI for Refs. 13 and 34 were inferred from graphical data assuming $C = 0$ and, therefore, do not represent the "best fit" to that data. Comparison with the low-energy stopping particle data is worse except for protons stopping in NE 102.[29] The large values of the parameter S for the Pilot U data[32] suggest that the results cannot be extrapolated to small values of dE/dx. Of course, differences in the types of scintillators employed may account for some of the variation in results, but it appears that a single theory of saturation, as represented by Eq. (A1), does not apply to both low-energy stopping particles with large ionization rates and relativistic nuclei.[30,32] Further, the data of Refs. 13 and 34 suggest that at high energy the saturation depends explicitly on the charge of the particle under study.

---

*Present address: The Enrico Fermi Institute, University of Chicago, Chicago, Illinois.
†Present address: Lawrence Berkeley Laboratory, Berkeley, California.
‡Present address: General Electric Corporate Research and Development, Schenectady, New York.

[1]H. H. Heckman, D. E. Greiner, P. J. Lindstrom, and F. S. Bieser, Science 174, 1130 (1971).
[2]H. H. Heckman, D. E. Greiner, P. J. Lindstrom, and F. S. Bieser, Phys. Rev. Lett. 28, 926 (1972).
[3]P. J. Lindstrom, D. E. Greiner, H. H. Heckman, B. Cork, and F. S. Bieser, Lawrence Berkeley Laboratory Report No. LBL-3650, 1975 (unpublished).
[4]D. E. Greiner, P. J. Lindstrom, H. H. Heckman, B. Cork, and F. S. Bieser, Phys. Rev. Lett. 35, 152 (1975).
[5]B. Jakobsson, R. Kullberg, and I. Otterlund, University of Lund, Cosmic Ray Physics Report No. LUIP-CR-75-02, 1975 (unpublished).
[6]J. M. Kidd, J. P. Wefel, W. Schimmerling, and K. G. Vosburgh, in *Proceedings of the Fourteenth International Conference on Cosmic Rays, Munich, 1975*, edited by Klaus Pinkau (Max-Planck-Institute, München, 1975), Vol. 2, p. 510.
[7]H. L. Bradt and B. Peters, Phys. Rev. 77, 34 (1950).
[8]T. Saito, J. Phys. Soc. Jpn. 38, 282 (1975).
[9]S. Barshay *et al.*, Phys. Lett. 51B, 5 (1974).
[10]R. Silberberg and C. H. Tsao, Astrophys. J. Suppl. 25, 315 (1973).
[11]A. S. Goldhaber, Phys. Lett. 53B, 306 (1974).
[12]M. G. White, M. Isaila, K. Prelec, and H. L. Allen, Science 174, 1121 (1971).
[13]W. R. Webber and J. Kish, Nucl. Instrum. Methods 99, 237 (1972).
[14]J. H. Adams, Jr., J. M. Kidd, R. Silberberg, and J. P. Wefel, in *Proceedings of the Thirteenth International Conference on Cosmic Rays, Denver, 1973* (Colorado Associated Univ. Press, Boulder, 1973), Vol. 1, p. 551.
[15]D. L. Cheshire, R. W. Huggett, D. P. Johnson, W. V. Jones, S. P. Rountree, S. D. Verma, W. K. H. Schmidt, R. J. Kurz, T. Bowen, and E. P. Krider, Phys. Rev. D 10, 25 (1974).
[16]R. J. Tapper, NIRL Report No. R-95, 1965 (unpublished).
[17]J. D. Jackson, *Classical Electrodynamics* (Wiley, New York, 1962), p. 455.
[18]A. Abdul-Magd and J. Hufner, Z. Phys. A277, 379 (1976).
[19]H. Masuda and F. Uchiyama, Phys. Rev. C 15, 972 (1977).
[20]W. Schimmerling, K. G. Vosburgh, K. Koepke, and W. Wales, Phys. Rev. Lett. 33, 1170 (1974).
[21]K. G. Vosburgh, W. Schimmerling, K. Koepke, and W. Wales, Phys. Rev. D 11, 1743 (1975).
[22]G. M. Raisbeck, J. Lestringuez, and F. Yiou, Phys. Rev. C 6, 685 (1972).
[23]P. Fontes, C. Perron, J. Lestringuez, F. Yiou, and R. Bernas, Nucl. Phys. A165, 405 (1971).
[24]F. Yiou, C. Seide, and R. Bernas, J. Geophys. Res. 74, 2447 (1969).
[25]F. Yiou, Ann. Phys. (N.Y.) 3, 169 (1968).
[26]G. M. Raisbeck and F. Yiou, in *Proceedings of the Thirteenth International Conference on Cosmic Rays Denver, 1973*, (Ref. 14), Vol. 1, p. 494.
[27]F. Yiou, G. M. Raisbeck, C. Perron, and P. Fontes,

in *Proceedings of the Thirteenth International Conference on Cosmic Rays, Denver, 1973,* (Ref. 14), Vol. 1, p. 512.
[28]J. F. Janni, Air Force Weapons Laboratory Technical Report No. AFWL-TR-65-150, 1966 (unpublished).
[29]D. E. Groom and M. G. Hauser, Nucl. Instrum. Methods 46, 301 (1967).
[30]L. Muga and G. Griffith, Phys. Rev. B 9, 3639 (1974).
[31]D. L. Smith, R. G. Polk, and T. G. Miller, Nucl. Instrum. Methods 64, 157 (1968).
[32]M. Buenerd, D. L. Hendrie, U. Jahnke, J. Mahoney, A. Menchaca-Rocha, C. Olmer, and D. K. Scott. Nucl. Instrum. Methods 136, 173 (1976).
[33]G. D. Badhwar, C. L. Deney, B. R. Dennis, and M. F. Kaplon, Nucl. Instrum. Methods 57, 116 (1967).
[34]W. R. Webber, J. A. Lesniak, and J. Kish, Nucl. Instrum. Methods 111, 301 (1973).
[35]J. B. Birks, *The Theory and Practice of Scintillation Counting* (MacMillan, New York, 1964).
[36]C. N. Chou, Phys. Rev. 87, 904 (1952).